Thin-Walled Structures 109 (2016) 103–112

Contents lists available at ScienceDirect

Thin-Walled Structures

journal homepage: www.elsevier.com/locate/tws

Buckling collapse of HDPE liners: Experimental set-up and FEM simulations

F. Rueda [a,*], A. Marquez [a], J.L. Otegui [a,b], P.M. Frontini [a]

[a] INTEMA, Instituto de Ciencia y Tecnología de Materiales, Universidad Nacional de Mar del Plata, B7608FDQ, Argentina
[b] Presently at Y-TEC (YPF - CONICET), Baradero 777, 1925 Ensenada, Argentina

ARTICLE INFO

Article history:
Received 2 February 2016
Received in revised form
14 June 2016
Accepted 9 September 2016

ABSTRACT

The purpose of this work is to provide a more complete framework for the development of short-term thermoplastic models to improve the design of liners subjected to external pressure. A device to perform short-term physical collapse buckling tests on HDPE liners to emulate in-service behavior under controlled conditions was designed and constructed. Tests were performed to explore the effect of temperature (in the range of 0–60 °C) on the buckling parameters of a HDPE pipe confined in a steel host pipe. The constitutive model for this material was calibrated from compression and tensile tests, performed at various strain rates and temperatures. The Three Network viscoplastic material constitutive model was adopted to reproduce material behavior. Full 3D FEM simulations of collapse buckling tests were conducted and validated against experimental data. Once the 3D full FE model was verified a simplified 2D model was generated to perform an intensive parametric study considering many temperatures and pipe aspect ratios. With data arising from the parametric study a predictive Glock's type function was derived, which takes into account the effect of temperature and the viscoplastic constitutive behavior of HDPE.

1. Introduction

1.1. Background to the technological problem

Relining deteriorated host pipes with polymeric liners has become an increasingly cost-effective popular method of pipeline rehabilitation. One of its main applications is for oil and gas pipelines. These liners serve the function of providing internal protection of metallic tubes mainly in two different situations; namely in providing enhanced corrosion resistance from aggressive chemical agents, and in rehabilitating already damaged pipelines [1].

In principle, any thermoplastic material can be used as a liner for oilfield pipelines. However, because of its relatively low cost, widespread availability, ease of production and installation and long history of service in oil and gas applications, HDPE (high density polyethylene) is the most frequently used thermoplastic for oilfield pipeline liners [2,3].

Despite HDPE liners are regularly used in the oil and chemical industry, they suffer one drawback: during normal operation gases present in the conveyed fluid permeate into the annulus volume between the liner and the host pipe. In the case of a sudden (intentional or accidental) loss of pressure, this can cause the liner to collapse due to external hydrostatic pressure if the wall thickness and the mechanical properties of the liner are not sufficient. When the external pressure is higher than the internal one, the liner will be subjected to a net external pressure that may destabilize the liner once the net pressure exceeds a critical value. This external pressure will induce deflections of the liner within the host pipe. To prevent liner collapse, the thickness of a liner must be chosen to resist this external pressure over the lifetime of the system [4].

Usually, buckling collapse of HDPE liners induced by external pressure takes place by the combined action of two separate factors: i) the permeation of oil derived gases through the liner wall for extended periods of time, and ii) the rapid decompression of pipelines that can occur during service stoppages or maintenance and inspection shutdowns [2,5].

Material failure is associated with the phenomenon known as physical swelling [2,6–11] which occurred when pipe grade thermoplastic is in contact with low molecular weight hydrocarbons (condensate) to result in a swell by weight of approximately 10%. At typical operating temperatures the gaseous components, such as the CO_2 and CH_4 dissolved in oil, aided by the high pressure operating conditions can permeate throughout the liner wall and gradually balance the pressure difference between the inside of the liner and the annular region or gap between the liner and the pipe wall. This permeation mechanism worsens recursively since permeation rate increases with the severity of liner swelling.

* Corresponding author.

http://dx.doi.org/10.1016/j.tws.2016.09.011
0263-8231/

Fig. 1. In-service liner buckling collapse.

Finally, buckling collapse occurs when the liner is decompressed and the external pressure, built up by the confined gases in the annular region, generates a stress state in the liner that induces the radial buckling failure. Fig. 1 depicts a typical one-lobe collapse. Hydrocarbon absorption causes reduction in modulus, which reduces the critical buckling pressure. HDPE liners are installed and operated at temperatures from 0 °C to 65 °C [2,12,13]; this effect is more severe at higher temperatures [2].

The depicted collapse phenomenon typically occurs within 1 h and it is called short-term collapse. Conversely, when constant loads are applied over a long time, log-term [4,14,15] or creep buckling occurs, this type of failure is beyond the scope of this paper.

Liners buckling resistance under short-term loads is typically examined by performing the so-called short-term tests [16]. In a short-term test a uniform external radial pressure is applied on a liner encased in a rigid chamber. The pressure is increased gradually until it reaches a maximum value known as collapse pressure or critical pressure (Pc). At this moment the liner collapses and pressure decreases while lobes volume increases.

The purpose of this work is to provide a more complete framework for the development of improved short- term liner design models. To this aim we designed and constructed a test device to develop short-term collapse buckling tests on HDPE liners under controlled conditions. Tests were performed to examine the effect of testing temperature (from 0 to 60 °C) on the buckling characteristics of a HDPE pipe confined in a steel host pipe.

The predictive capacity of a recently obtained mathematical procedure for the calculation of buckling pressure under viscoplastic regime [17,18] is evaluated by comparing predictions with laboratory testing. This mathematical procedure combines FEM structural simulation with Three Network viscoplastic material constitutive model [19]. Material behavior was calibrated from compression and tension tests data determined at various strain rates and temperatures.

Full 3D FEM simulations were conducted and validated against experimental buckling collapse data. Once the validity of the model was univocally verified, simplified 2D simulations were also carried out and recursively validated against full 3D simulations. Based on these 2D simulations, an intensive parametric study considering many temperatures and pipe thickness-to-diameter aspect ratios (W/t) was conducted. From the obtained parametric data, a predictive Glock's type function [20] was constructed which takes into account the effect of temperature and the viscoplastic constitutive behavior of HDPE. We believe that this model could be used in the future to represent long term behavior as well.

1.2. Prediction of time-temperature dependent buckling collapse pressure

In recent years a considerable amount of research has been undertaken to better understand and quantify the structural performance of lined pipe systems [14–16,21–31]. Although existing design methodologies do recognize the importance of liner buckling, they have been extensively criticized for being too simplistic [26].

Most of the earlier studies for the instability of liners were only concerned with elastic instability and did not consider any material inelasticity or plasticity [31]. Therefore, those studies may help in estimating the buckling pressure of thin liners that are only expected to buckle elastically, prior to any material yielding. However it is known that material yielding would affect the mechanical and buckling behavior of liners [23].

One of the main shortcomings regarding modeling HDPE liners performance is the intrinsic non linearity of polymer behavior [32]. In contrast with steel which exhibits well-defined material yielding, polymers have no well-defined yield stress and their mechanical behavior is time dependent.

The non-linear characteristics of the problem generate convergence issues that make it difficult for classical FEM to reproduce experimental behavior. Moreover, these models are not adequate to reproduce the complex multiaxial stress response and rate-dependent deformation evolution that will take place during an actual rapid pipe depressurization situation. Consequently, a different approach was devised and implemented in previous investigations [17,18,33] by the authors. On one hand we demonstrated the pertinence of using fluid elements in finite element modeling (FEM) to simulate collapse buckling of confined liners. This innovative approach allowed simulating the post-collapse pressure drop, to reproduce dynamic loading histories and to incorporate time-dependent material constitutive models. The hydrostatic elements introduced by the authors enabled FEM modeling of the whole process of elastic and inelastic collapse of polymer liners, under dynamic or static conditions.

On the other hand, it was also shown that an advanced viscoelastic–viscoplastic model available in literature, the so-called Three Network Model, TNM, [19] is able of reproducing the complex mechanical response of an HDPE liner at different loading rates [17,18]. The strain rate and pressure dependent mechanical response of HDPE liners was assessed by modeling the buckling collapse dynamic event as an increasing volume of fluid entering the gap cavity between liner and host pipe. It was found that the material strain rate dependency has a significant effect on the collapse pressure (Pc). The influence of w/D in the non-linear inelastic bucking behavior was established, thus extending El Sawy analysis [23] to time dependent materials.

In the present paper the constitutive TNM model's performance is directly assessed by comparing experimental and predicted failure pressures of HDPE liners, confined in a steel host pipe pressurized to failure at different environmental temperatures.

2. Experimental

Theoretical and numerical treatments in principle enable the development of improved design procedures, however, there is an acute shortage of good quality physical test data in the literature with which to verify and calibrate the mathematical models. So that a device was designed and constructed in order to generate a physical collapse of HDPE liners.

2.1. Materials

One meter long HDPE tubes with 0.054 w/D aspect ratio (114 mm outside diameter and 6.2 mm wall thickness) were used for calibration of constitutive models and buckling collapse tests. Pipe samples were processed with HDPE DGDA 2490, kindly provided by DOW.

2.2. Testing setup for experimental collapse of liners

The layout of the apparatus shown in Fig. 2, main parts and working principle are represented in the schematic diagram of Fig. 3. Briefly, the equipment consists of a steel host pipe swage-lined with the plastic "liner" to be tested.

The device allows progressively increasing pressure in the interstice between the pipe and the liner, up to achieving the collapse of the latter. The pressure within the inner volume of the liner is maintained constant and equal to atmospheric pressure, so that the interstitial volume must be confined and sealed separately from the inner volume of the liner. This generates the necessary pressure difference between the outside and the inside of the "liner" to achieve collapse.

A key consideration in the design of the device was the need to emulate the same plane strain condition to which liners are subjected in service. This is associated to the fact that liners are installed in lengths that range from 200 to 1200 m [34]. This suppresses boundary conditions of the endings of the liner in the collapsed area. As a primary approximation, in order to meet the minimum length needed to reproduce this effect, finite element modeling and simulation of collapse were done at different pipe lengths assuming a perfect elasto-plastic material behavior as in our first paper [33]. We observed an asymptotic trending to plane strain condition with increasing pipe length, as shown in Fig. 4.

For a length of the pipe above four times its diameter (in this case, about 0.45 m), the results are independent of length. Under these considerations the devise was designed to accommodate a one meter long liner. A 14 mm thick seamless tube was used; its bore was machined to achieve a controlled interference with the outer diameter of the liners. Four circumferentially distributed ¼ BSP connections were provided in the central part of the tube to communicate interstitial pressure. The design of sealings (Fig. 5) at pipe endings contemplates the need for suppressing longitudinal restraint to the liner. This was achieved using O-rings confined between flanges and pipe, in 45 degree conical seats.

Fig. 2. Liner insertion system for buckling collapse tests.

A system to insert the liner within the hosting pipe using the technique known as swagelining (Fig. 2) was also designed. Two API 150 flanges serve as structural elements for fixing the rig and tension the "liner" during the insertion procedure, while ensuring gap sealing. The inner diameter of the insertion side flange is smaller than the other flange, to secure the swaging process by Poisson effect during insertion. Four threaded rods connect both flanges to preload the assembly, and their tips serve as fixing bolts for the pulling rig. The rig is long enough for the liner to be extracted out of the hosting pipe once finished the test.

Numerical simulation reproducing test conditions showed that maximum insertion load for the liner is, roughly, 12,000 N. This value, with an appropriate safety factor, was used to dimension the loading structures. A winch was used to exert the load through a pulling head that ensures load concentricity and uniform distribution,.

The test procedure included increasing the external pressure exerted on the "liner" by pumping water into the gap until collapse. Interstice (gap) pressure and the evolution of the water volume during were continuously measured using digital gauges during the buckling process.

Tests at different temperatures were conducted in a thermostatic water bath). Predetermined temperatures were maintained either by controlled direct injection of steam into the bath or by adding ice. All test times were within the so-called "short term" regime, that is a loading time no longer than 30 min [16]. Sample number, test temperature, and total test time are summarized in Table 1.

2.3. Uniaxial tensile and compression tests

Constitutive material behavior was determined by performing, tensile and compression tests on an Instron 4467 universal testing machine. Tensile and compression specimens were machined out from a supplied liner (Fig. 6); nine specimens for each loading case were used. Tests were carried out at 3 different cross head speeds and 4 different temperatures, according to the configuration shown in Table 2.

Tensile tests were performed in 2.5 mm × 2.5 mm cross-section dogbone-shaped specimens (remaining dimensions correspond to type V^C specimens in ASTM D638-03 [35]). Compression tests were carried out in 10 mm long, 5 mm diameter specimens, following the 2:1 (height: diameter) ratio recommended in [36]. For a complete characterization of deformation evolution, both loading and unloading responses were recorded at each temperature.

3. Computational modeling

3.1. Material constitutive model

In what follows the main features of the Three Network model, TNM, adopted as constitutive framework for through this work are described. More details on the formulation can be found in the original works [19,37] and in our previous paper [17]. The TNM model consists of three networks acting in parallel. A simplified one-dimensional rheological representation can be seen in Fig. 7.

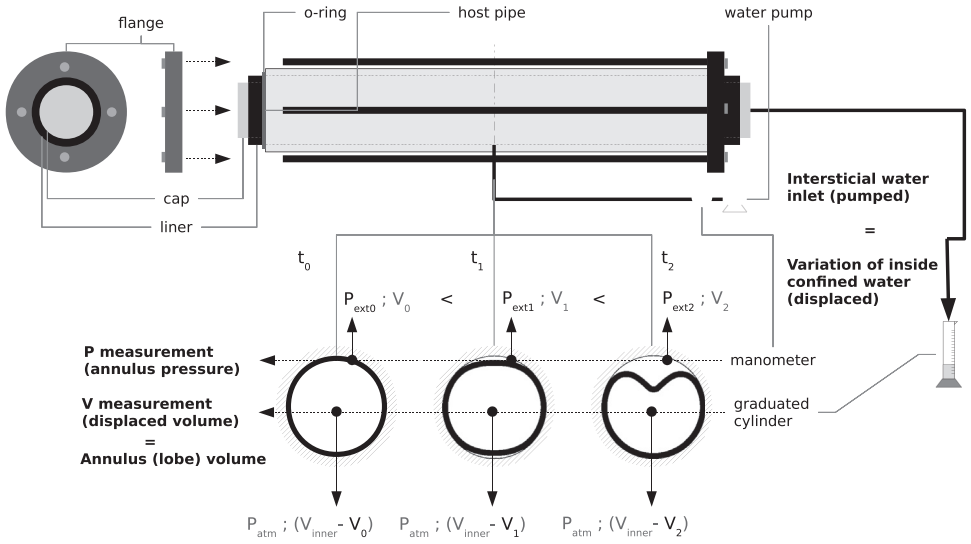

Fig. 3. Schematic diagram of liners buckling tests setup.

Networks A and B represent the initial viscoplastic response, which is captured using two separate energy activation deformation mechanisms corresponding to amorphous and semicrystalline domains of the polymer. Network C captures the overall non-viscous hyperelastic component of the material response, i.e. the entropic chain stretch hardening. The total deformation gradient (F^{app}) of the assembly is decomposed into a thermal expansion component (F^{th}) and a mechanical deformation component (F):

$$F^{app} = FF^{th} \tag{1}$$

The mechanical deformation gradient of networks A and B are further decomposed into elastic and viscoplastic components:

$$F = F_n^e F_n^v \tag{2}$$

Where n takes the value A and B, for networks A and B correspondingly. F_n^e is the elastic component of the deformation gradient, which is constitutively determined from Eq. (3). F_n^v is the viscoplastic component of **F** and is constitutively determined from Eqs. (5) and (6).

The Cauchy stress acting in networks A and B has the following form:

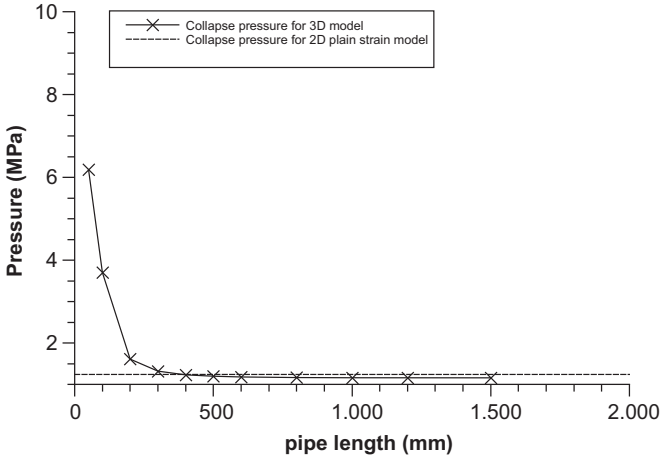

Fig. 4. Buckling collapse critical pressure as a function of pipe length obtained by FEM assuming a perfect elastic-plastic material behavior.

$$\boldsymbol{\sigma}_n = \frac{\mu_n}{J_n^e \bar{\lambda}_n^{e*}}\left[1 + \frac{\theta - \theta_0}{\hat{\theta}}\right]\frac{\mathcal{L}^{-1}\left(\bar{\lambda}_n^{e*}/\lambda_L\right)}{\mathcal{L}^{-1}\left(1/\lambda_L\right)}\mathrm{dev}\left[\mathbf{b}_n^{e*}\right] + \kappa\left(J_n^e - 1\right)\mathbf{1} \tag{3}$$

Where, $J_n^e = det\left[F_n^e\right]$; $\mathbf{b}_n^{e*} = (J_n^e)^{-2/3}\mathbf{F}_n^e(\mathbf{F}_n^e)^{\mathrm{T}}$ is the Cauchy-Green deformation tensor; θ is the current temperature; θ_0 is a reference temperature; $\hat{\theta}$ is a material parameter specifying the temperature response of stiffness; $\bar{\lambda}_n^{e*} = (\mathrm{tr}[\mathbf{b}_n^{e*}]/3)^{1/2}$ is the effective chain stretch and $L^{-1}(x)$ is the inverse Langevin function; μ_n is the elastic shear modulus of network n and κ is the bulk modulus. These material constants can be interpreted as analogous to the linear elastic shear and bulk modulus, with the difference that in the TNM model the shear modulus is scaled by the Langevin function. λ_L is the locking stretch and gives a measure of the hyperelastic hardening response at large strains.

The velocity gradient of networks A and B have the following form:

$$\dot{\mathbf{F}}_n^v = \dot{\gamma}_n \mathbf{F}_n^{e-1}\frac{\mathrm{dev}\left[\boldsymbol{\sigma}_n\right]}{\tau_n}\mathbf{F} \tag{4}$$

Where the flow rate $\dot{\gamma}$ is given by a power-law flow equation:

$$\dot{\gamma}_n = \dot{\gamma}_0\left(\frac{\tau_n}{\hat{\tau}_n + aR\left(p_n\right)}\right)^{m_n}\left(\frac{\theta}{\theta_0}\right)^n \tag{5}$$

Here $\dot{\gamma}_0\left[\frac{1}{s}\right]$ is a constant introduced for dimensional consistency, $R(x)$ is the ramp function; p_n is the hydrostatic pressure; $\square_n$ is the Frobenius norm of the deviatoric part of $\square_n$; τ_n is the flow resistance of network n and gives a measure of the shear stress at which plastic flow becomes a dominant deformation mechanism; m is the stress exponential of the power-law equation and mainly determines the material strain-rate sensitivity.

The Cauchy stress acting in network C has the following form:

$$\boldsymbol{\sigma}_C = \frac{1}{1+q}\left\{\frac{\mu_C}{J\lambda_{chain}}\left[1 + \frac{\theta - \theta_0}{\hat{\theta}}\right]\frac{\mathcal{L}^{-1}\left(\lambda_{chain}/\lambda_L\right)}{\mathcal{L}^{-1}\left(1/\lambda_L\right)}\mathrm{dev}\left[\mathbf{b}^*\right] + \kappa\left(J-1\right)\mathbf{1} + q\frac{\mu_C}{J}\left[I_1^*\mathbf{b}^* - \frac{2I_2^*}{3}\mathbf{I} - \left(\mathbf{b}^*\right)^2\right]\right\} \tag{6}$$

where $J = \det[\mathbf{F}]$; $\mathbf{b}^* = J^{-2/3}\mathbf{F}(\mathbf{F})^{\mathrm{T}}$is the Cauchy-Green deformation tensor, and $\lambda_{chain} = (\mathrm{tr}[\mathbf{b}^*]/3)^{1/2}$.

Finally, since they are in parallel, the three networks have equal mechanical deformation gradients and the total stress of the system is the sum of each network stress.

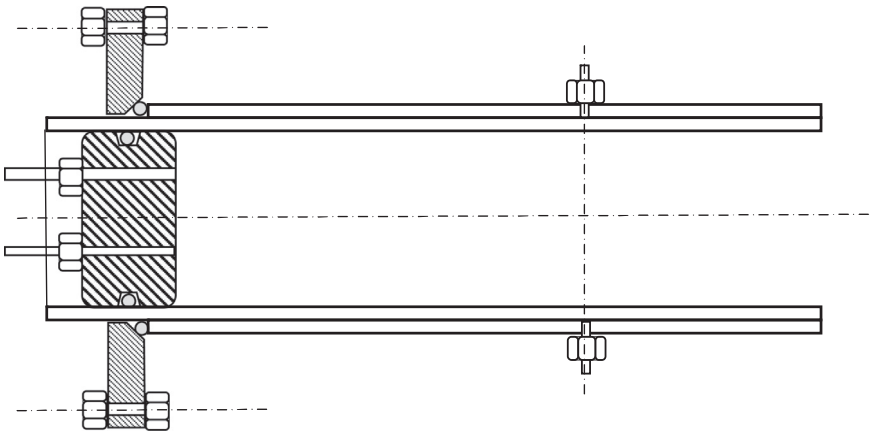

Fig. 5. Detail of sealing design.

Table 1
Buckling collapse test conditions.

Liner	Temperature °C (K)	Test duration (min)
1	24 (297)	15
2	61 (334)	10
3	58 (331)	10
4	32 (305)	15
5	4 (277)	15

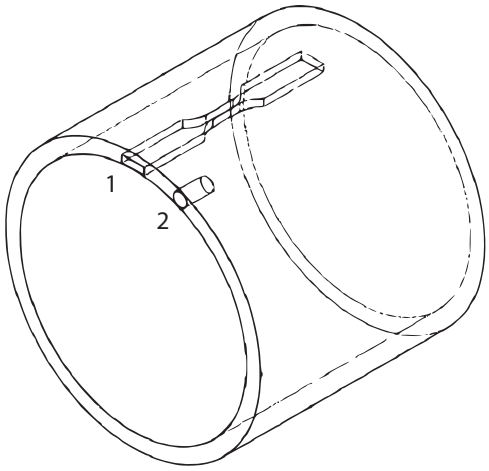

Fig. 6. Tension (1) and compression (2) specimens as machined from the original pipe.

The TNM model was executed as a user material subroutine (UMAT/VUMAT) for ABAQUS using the PolyUmod material libraries [38].

3.2. Constitutive model calibration

Model parameters calibration was performed using uniaxial tensile and compression experimental data specifically determined for this purpose (see experimental section). The constitutive parameters were determined using a parameter-extraction software, namely MCalibration [39], which enables semi-automatic extraction of material parameters using as input different loading cases (monotonic, dynamic mechanical analysis, creep, etc.) with several loading modes (uniaxial, biaxial, plane stress, etc.) for a variety of advanced constitutive models, including the TNM model. This software determines parameter values using a minimization algorithm based on the Nelder-Mead simplex method [40]. This method uses iterations to evaluate the difference between the model predictions and the experimental results in a least-squares sense, i.e. using a minimum squares cost function. In each iteration, the method tries a new estimation for the constitutive parameters using an approximation criterion and the iterations continue until the cost function reaches an established minimum. Initial values and upper and lower bound values for the optimization method are already predefined in the calibration software using typical thermoplastic material constitutive parameters [19].

3.3. Numerical simulation of collapse buckling test

3.3.1. Full 3D FEM simulations

Buckling collapse tests were simulated by FEM model in ABAQUS/Standard 6.10 using the TNM model. The FEM model was performed in a 3D simplified geometry of a quarter of the original as showed in Fig. 8a. A small elliptical curvature (i.e. a 0.4% difference between the lower-half y-radius and the upper-half y-radius values) was introduced in the upper part of the liner along the y-axis in order to induce single lobe buckling (Fig. 1) in this region. Single lobe buckling is considered the most critical failure mode and the most frequently observed in practice.

The thermoplastic liner was modeled using C3D20R elements and assuming the steel pipe holder as a discrete rigid. The fluid was modeled using F3D3 hydrostatic fluid elements and the depressurization event was modeled by imposing a fluid volume flux using the “fluid flux” option in ABAQUS/Standard. A classical static FEM analysis would have involved imposing a continuously increasing pressure on the outer liner surface. However, for the present analysis, this approach typically fails at the peak (i.e. buckling) pressure. In other words, pressure evolution in the cavity cannot be imposed beforehand as an independent variable. Therefore, the fluid volume flux approach is more pertinent since it models the real cause of pressure increase, i.e. the entrance of a fluid into the annulus. An example of the application of this method in modeling liner buckling collapse can be found in [33]. The hydrostatic fluid elements are surface elements that cover the boundary of the fluid-containing cavity and provide the coupling between the deformation of the fluid-filled solid and the pressure exerted by the contained fluid on the solid surface defined as cavity boundary [41].

Prediction capabilities of these simulations are validated against physical collapse experiments. Thus, simulations were run for every of the three temperatures selected for the physical collapse experiments. The imposed fluid volume flux in FEM model

Table 2
Uniaxial tensile and compression tests: temperature and cross head speed conditions.

	273 Kº		298 Kº		333 Kº		353 °K	
Cross head speed	T	C	T	C	T	C	T	C
1 mm/min								
10 mm/min								
50 mm/min								

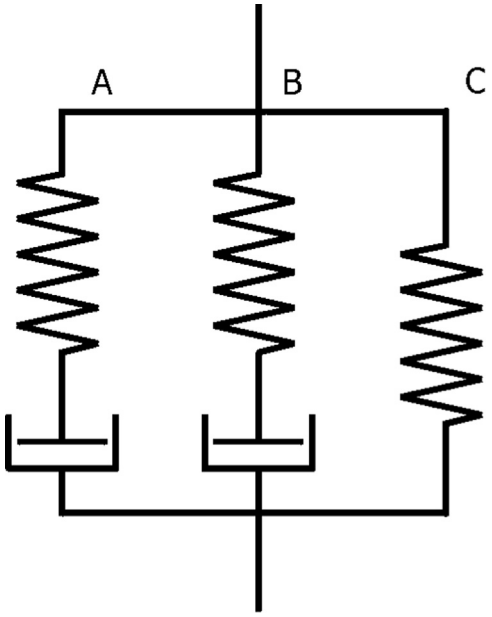

Fig. 7. Rheological one-dimensional representation of the TNM constitutive model.

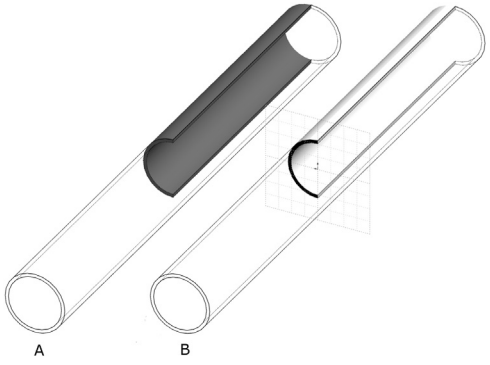

Fig. 8. Simplification of FEA by symmetry for 3D (A) and 2D (B) models.

was 130 cm^3/min, approximately the same fluid volume flux of the physical experiment, to achieve in both cases a total test time between 10 and 15 min. The latter procedure allows to univocally validate $3 \cdot D$ FEM geometric simulation and TNM constitutive model as illustrated in Section 4.3.

3.3.2. 2D FEM simulations and parametric analysis

With the aim of exploring the influence of temperature and aspect ratio (w/D) on Pc, a numerical parametric analysis was performed. Simpler 2D FEM simulations were executed and their pertinence verified against full 3D FEM simulations. In the 2D situation a unit length strip of the liner is only considered because of the long cylindrical geometry of the liner (i.e. plane strain conditions prevail) and half of the liner is only modeled due to symmetry (Fig. 8b). The thermoplastic liner is now considered to be a planar bidimensional deformable solid using CPE8R elements and assuming plain strain conditions, i.e. neglecting the effect of restraint at the liner ends. This assumption has proven to be valid for length to radius values greater than 6 [42]. A small elliptical curvature (i.e. a 0.4% difference between the lower-half y-radius and the upper-half y-radius values) was introduced in the upper part of the liner along the y-axis in order to induce single lob buckling. The external metallic tube was assumed as discrete rigid and the fluid was modeled following the same approach as 3D model but using F2D2 bi-dimensional hydrostatic fluid elements. The aspect ratio was varied from 0.03 to 0.11 and the temperature with an increment of 0.015 to cover some practical ranges involving thin and thick liners. The temperature was varied from 265 K° to 345 K° with an increment of 10 K° to cover practical operating range [2,12,13].

4. Results

4.1. Uniaxial tensile and compression tests

Tensile and compression tests results at different strain rates and temperatures are shown together in Fig. 9. Stress-strain traces are presented for 1, 10 and 50 mm/min cross-head speeds and temperatures of 273, 298, 333 and 353 K. Points and solid lines are experimental and model prediction values, respectively.

At a stress value between 5 and 10 MPa the material enters the visco-elastoplastic regime, this region corresponds to the complex onset of different plastic flow mechanisms in the amorphous and semicrystalline domains of the thermoplastic material [19,37]. In the constitutive model, the deformation gradients of the dashpots, which were at first negligible, start to flow at these stress values. Also in this regime, hardening is observed with increasing the strain rate and decreasing temperature, as expected. The material shows strain rate and temperature sensitivity both in tension and compression. When increasing the crosshead speed from 1 mm/min to 50 mm/min at constant temperature of 298 °K, a ≈ 30%

increase in the value of the maximum attained stress can be observed. At constant crosshead speed of 1 mm/min, when decreasing temperature from 353 °K to 273 °K, ≈400% increase in the value of the maximum attained stress can be observed. Pressure dependency can be observed as the maximum stress achieved in compression is higher than in tension for equal deformation rates. For the TNM model, a very good fit was obtained between experimental and TNM model predictions, with a R^2 (Coefficient of Determination) value of 0.976. The constitutive parameters obtained for the TNM model are presented in Table 3.

4.2. Physical buckling collapse tests

A single lobe collapse mode was verified for all of the buckling collapse tests, as showed in Fig. 10. As expected, due to the effect of restricted ends, the lobes appeared always in the middle of the liner. Furthermore, there was no preferential angular lobe location in the liner. This clearly indicates that there are no defects induced by the steel host pipe contact.

Pressure and cavity volume data were recorded continuously during all buckling tests, for each of the three temperatures, and then plotted together as depicted in Fig. 11. Deformed geometries obtained by FEM simulations are showed at four stages of collapse, indicated by arrows over each curve. Irrespectively of the test temperature, all of the curves display the typical shape already reported for short-term buckling collapse test [27].

As expected, pressure increases with the increase in the cavity volume up to a maximum value corresponding to the collapse pressure, Pc. A linear trend is only evident at low volumes. After this maximum an abrupt drop of pressure was verified and a subsequent asymptotic decrease of pressure was detected in correspondence with lobe propagation. The influence of temperature on the phenomenon is evident to the naked eye. The lower the temperature, the higher P_c and the steeper the slope value.

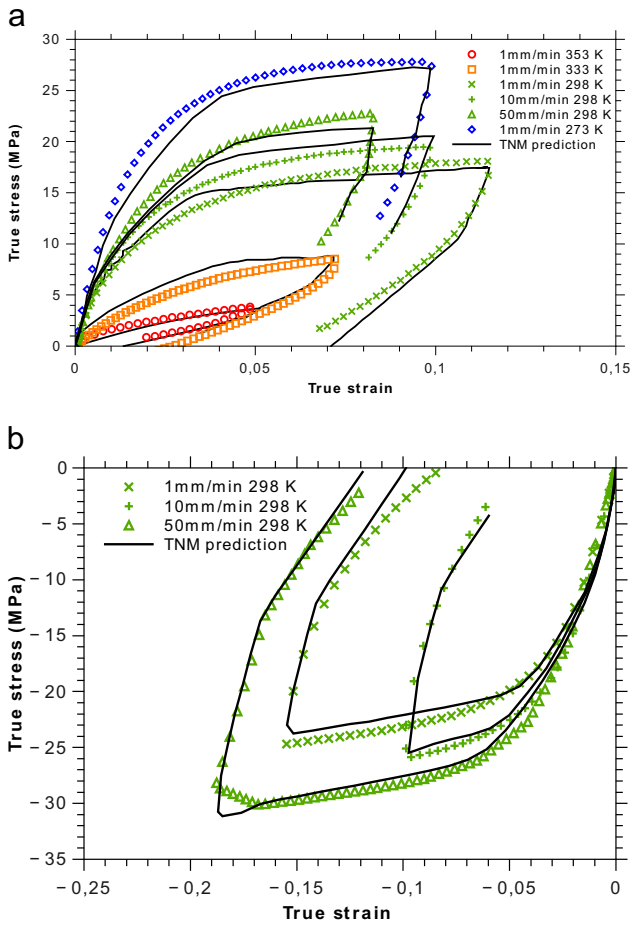

Fig. 9. HDPE uniaxial tensile (A) and compression (B) stress-strain traces.

Table 3
Constitutive parameters for TNM model.

Symbol	Name	Value
μ_A	Shear modulus of network A	212.16 MPa
λ_L	Chain locking stretch	2.12
$\hat{\theta}$	Temperature response of stiffness	−92.72 K
κ	Bulk modulus	2000 MPa
$\hat{\tau}_A$	Flow resistance of network A	5.78 MPa
a	Pressure dependence of flow	0.45
m_a	Stress exponential of network A	13.1
m_b	Stress exponential of network B	22.37
n	Viscosity parameter	117.18
$\hat{\tau}_B$	Flow resistance of network B	21.43 MPa
μ_{Bi}	Initial shear modulus of network B	255.8 MPa
μ_{Bf}	Final shear modulus of network B	120.3 MPa
μ_C	Shear modulus of network C	10.79
q	Relative contribution of I_2 of network C	0

4.3. Numerical simulation of buckling collapse tests: 3D full FEM

Fig. 11 also shows the results of numerical simulations plotted together with data recorded during physical buckling collapse tests. Traces show pressure evolution against the increase of cavity volume while FEM frames depicting geometry evolution during collapse test. As in physical tests, all numerical simulations showed one lobe collapse buckling. Fig. 12 (a) shows a simplified deformed geometry as used in FEM model. Fig. 12 (b) shows a mirror pattern of (a), for a cross-cut view of buckling at the middle of the liner.

An excellent agreement between simulations and physical experimental results (single points in the Fig. 11) was found. Only small discrepancies of 4,4% for 4 °C, 8% for 24 °C and 1% for 61 °C were found for P_c, considering percentage difference as P_c (experimental)/Pc(numerical)*100. These excellent results serve as a verification of the predictive quality of the TNM constitutive model for HDPE engineering applications.

4.4. Parametric analysis

The 2D FEM results of the parametric study are presented in this section. As stated in the “computational modeling” section, the 3D problem was approximated by a simplified 2D analyses assuming plane strain conditions and symmetry. To check the validity of 2D assumptions Pc values are compared in Table 4. Maximum discrepancies of 5.7% were measured between 3D and 2D FEM P_c values.

Two sets of parametric contour curves were then constructed using the 2D approximation. In Fig. 13a P_C (log) is plotted against temperature at constant w/D ratios while in Fig. 13b P_c (log) is plotted against w/D ratio for every tested temperature. Experimental data points (hollow points in Fig. 13) are plot together with simulated data which further support the validity of our predictions.

The parametric analysis performed for pipes having different w/D relationships showed a linear decreasing trend of Pc with temperature in the semilogarithmic plot (Fig. 13a). Then, the

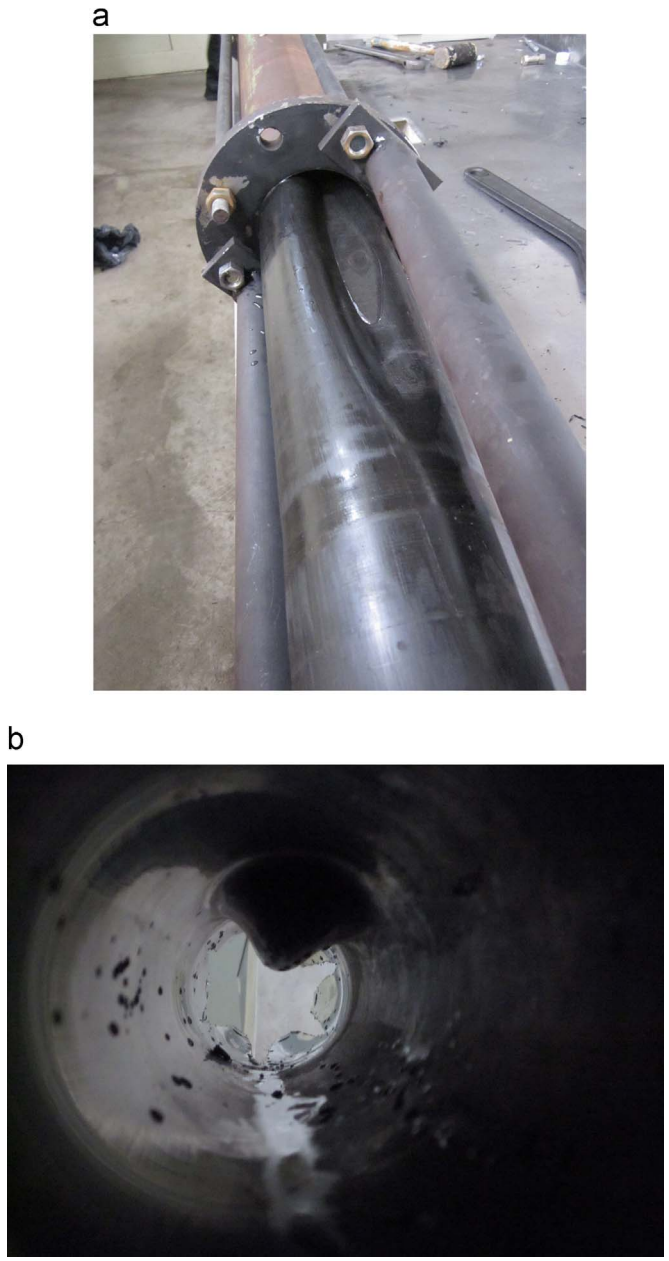

Fig. 10. Collapsed liner after laboratory buckling collapse test: a) while the pipe is extracting outside the host steel pipe b) an inside view.

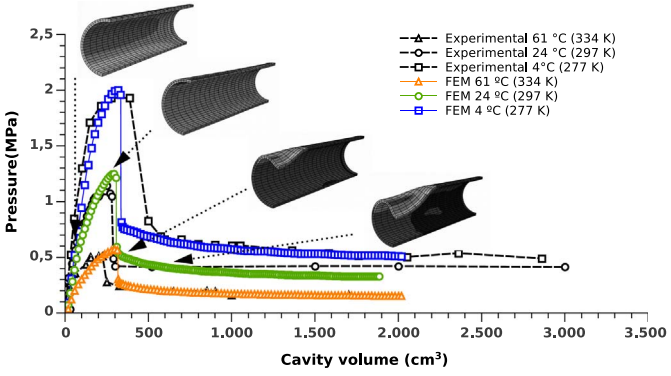

Fig. 11. Buckling collapse curves. Dotted and solid lines are experimental and predicted FEM results respectively.

P_c(T) contour lines corresponding to each $(w/D)_i$ values may be fitted to an exponential function. It is also noted that the resulting lines are nearly parallel. This justifies the use of a common scale parameter, for different aspect ratios.

Conversely, P_c (log) vs. w/D plot shows an increasing curvilinear trend at every temperature. This suggest that data condensed in Fig. 13b can be fitted to a single power law since curves are also nearly parallel.

In 1977 [20], Glock derived an analytical expressions relating buckling pressure with pipe geometry (w/D) valid within the elastic regime,

$$P_c = \frac{E}{1-\upsilon^2}\left(\frac{w}{D}\right)^{2.2} \tag{7}$$

Inspired in this famous relation we derived a Glock-like relation by fitting the data arising from the parametric study to Eq. (8) as follows:

$$P_c(T, w/D) = S(T)\left(\frac{w}{D}\right)^{C} \tag{8}$$

The C parameter was calibrated from data at constant temperature condensed in Fig. 13 (b)). A value of 1.95 was determined for this particulate case.

The parameter S(T) involves temperature dependent stiffness of the system and it can be calculated from data condensed in Fig. 13 (a)) as follows:

$$S(T) = \frac{P_c(T, (w/D)_0)}{\left((w/D)_0\right)^{C}} \tag{9}$$

$(w/D)_0$ is a reference aspect ratio and $P_c(T)$ is the critical pressure expressed as a function of temperature at $(w/D)_0$. Taking any w/D value as reference, $S(T)$ is calibrated by scaling curves to the reference value

$$S(T) = 4.37x10\ \ e^{\left(\frac{-T}{42.09}\right)} \tag{10}$$

Then, from Eq. (8) a full expression of the equation relating P_c, T and (w/D) was developed:

$$P_C\left(\frac{w}{D}, T\right) = S(T)\left(\frac{w}{D}\right)^{1.95} \tag{11}$$

Where P_c is the buckling collapse critical pressure expressed in Mpa, T is the test temperature expressed in K and (w/D) is the aspect relation of the pipe.

Eq. (11) is plotted in a 3D XYZ graph. Both P_c values arising from physical and FEM experiments are plotted together in Fig. 14 (a).

Predictions by Eq. (11) and the original Glock equation are contrasted against physical and FEM data harvest for the three temperatures of physical collapse buckling test in Fig. 15. Young's modulus values used in Glock equation were those determined in the uniaxial tensile experiments at each individual temperature (Fig. 9). This figure clearly shows that Glock equation overestimates *Pc*, consistently with the idea that collapse buckling of HDPE liners is highly inelastic [17,18,33] whereas, Glock equation only considers elastic deformations. Nevertheless, it can be appreciated that Glock predictions become more accurate at lower temperatures and low *w/D* ratios, for which less inelastic deformations are developed.

5. Conclusions

Short-term collapse buckling phenomena of HDPE liners confined in a steel host pipe was explored in this work. Tests undertaking increasing external pressure to failure were physically

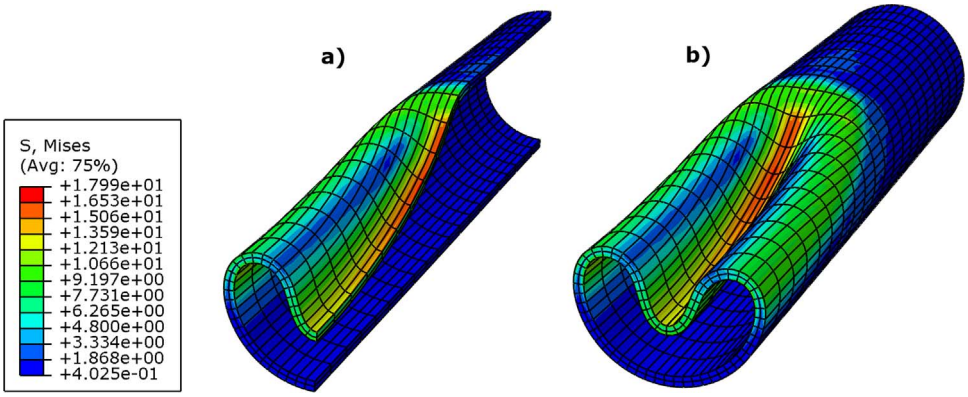

Fig. 12. Von Misses stress contours of deformed geometry obtained by FEM simulation The box on the left side shows color references of Von Mises stress values. (For interpretation of the references to color in this figure legend, the reader is referred to the web version of this article.)

Table 4
Comparison between 2D and 3D FEM simulations results.

Temperature (K)	P_c (MPa)		
	Experimental	FEM 2D	FEM 3D
277	1.94	2.1	2
297	1.14	1.17	1.22
334	0.53	0.58	0.55

performed and then, simulated using FEA. The main outcome of this research is the developing of a predictive mathematical procedure for the calculation of buckling pressure under viscoplastic regime.

Material constitutive response was determined from compression and tension tests performed at various strain rates and temperatures. As in previous work, a Three Network viscoplastic constitutive model was adopted [17].

The effect of testing temperature (from 0 to 60 °C) in the buckling characteristics of a HDPE pipe confined in a steel host pipe was examined. Critical buckling collapse pressure resulted highly dependent of test temperature, decreasing four times between 0 °C and 60 °C respectively.

Full 3D FEM simulations of the short-term (less than 30 min) collapse buckling experiments were conducted and validated against experimental data. The laboratory tests exhibited an excellent correlation with the theoretical predictions. So, this paper serve as a univoque verification of the predictive quality of Three Network viscoplastic constitutive model for HDPE pipe engineering applications [17,18]. From these results it also emerges that hydrostatic elements first introduced by us [33] is a suitable FEM tool for time-dependent problems allowing to reproduce the whole collapse event and not only the critical pressure.

In addition, in-service plane strain conditions were verified comparing results of complete 3D buckling collapse test simulation with planar bidimensional simulation assuming plain strain conditions. This allowed to use simplified 2D simulations as predictive tool. A parametric analysis were conducted by using 2D simulations at many temperatures and aspect ratios. Parametric results were used to modify Glock's elastic solution in order to represent HDPE liners viscoplastic behavior. The proposed equation is capable of predicting critical collapse pressure taking into account for the effect of temperature, strain rate and aspect ratio. This relationship may be very useful at the time of designing new polyethylene liners since it only requires the knowledge of material constitutive response.

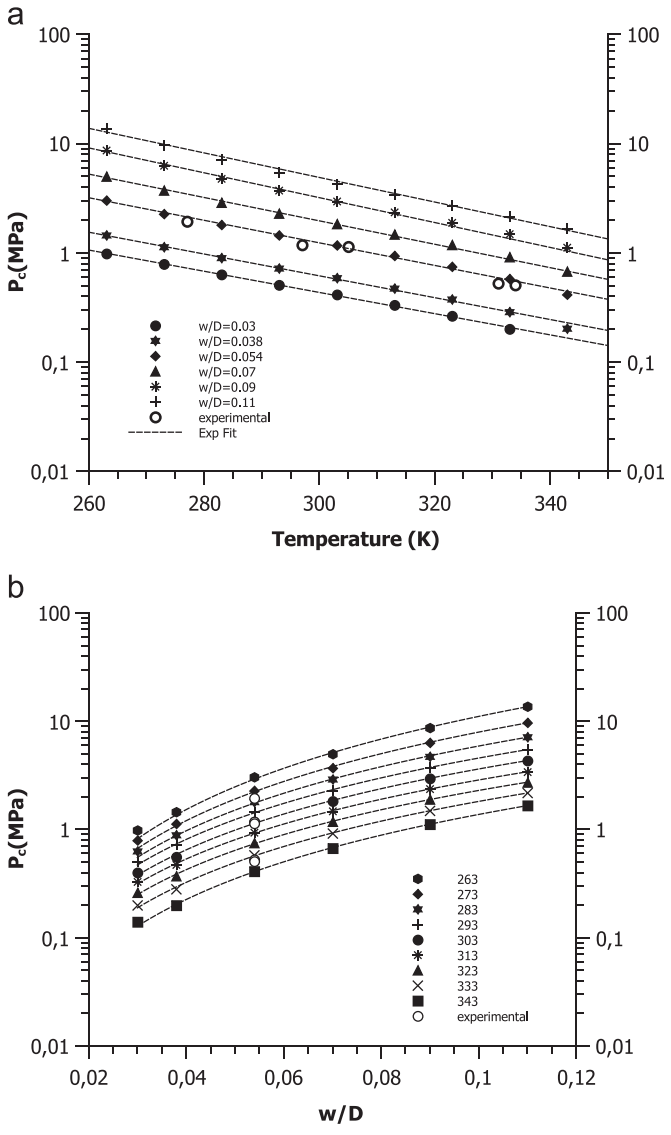

Fig. 13. P_c (log) against temperature (a) and P_c (log) against aspect ratio. Hollow and solid points are physical experimental results and numerical experimental results respectively; dotted lines are numerical results fittings.

We believe that mathematical procedure developed could be used in the future to represent long term behavior as well.

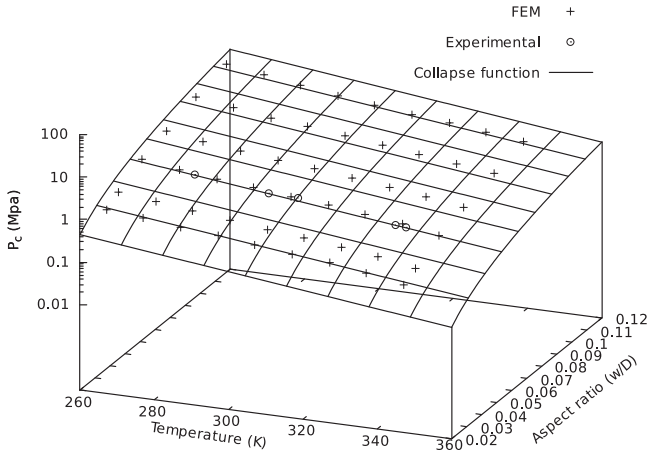

Fig. 14. P_c (log) against temperature and aspect ratio. Hollow points and crosses are physical and numerical results respectively; solid lines are the graphical representation of Eq. (11).

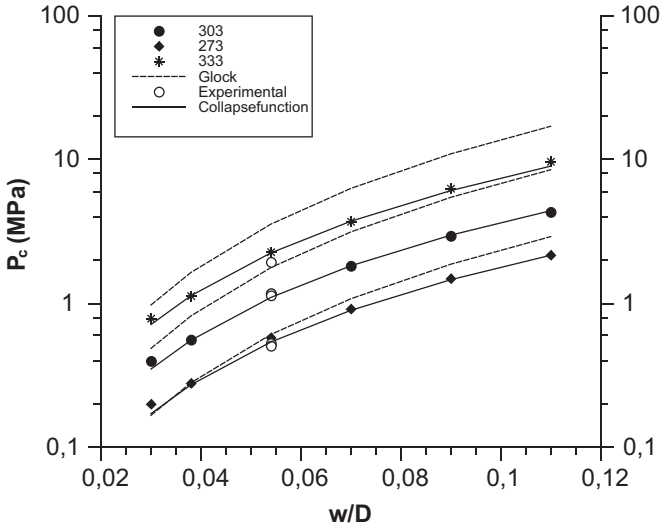

Fig. 15. P_c physical and numerical results against aspect ratio.

Acknowledgements

This research work was partly funded by CONICET (Consejo Nacional de Investigaciones Científicas y Técnicas de la República Argentina), Grant PIP 00193/12, and by Agencia de Promoción Científica (argentina), Grant PICT 0582/10. Authors thank Dow for kindly supplying material.

References

[1] E. Engle, Pipe Rehabilitation with Polyethylene Pipe Liners (No. HR-370), 2003.
[2] Jim Mason, Thermoplastic liners for oilfield pipelines, in: R.W. Revie (Ed.), Oil and Gas Pipelines: Integrity and Safety Handbook, John Wiley & Sons, Hoboken, New Jersey, 2015, pp. 449–451.
[3] ⟨http://www.aldyl.com.ar/petroleo.php⟩.
[4] M. Zhu, D.E. Hall, Creep induced contact and stress evolution in thin-walled pipe liners, Thin-Walled Struct. 39 (11) (2001) 939–959.
[5] Canadian Standards Association, CSA Z662-03 Oil and Gas Pipeline Systems, 2003.
[6] W. Woishnis,, S. Ebnesajjad, Chemical Resistance of Thermoplastics, William Andrew, Waltham USA, 2011.
[7] J.J. Baron, L.C. Macleod, K.E. Szklarz, Non-Metallic Liners for Gas/Condensate Pipelines, in: Proceedings of Corrosion 2000, NACE International.
[8] J.D. Alkire, Effect of Rapid Decompression Conditions on Liner Materials, in: Proceedings of Corrosion 2000, NACE International.
[9] M. Genoni, B. Bulleri, A. Ticci, J. Sutherland, Engineering Thermoplastic-Liners, in: Proceedings of Corrosion 2004, NACE International.
[10] C.J. Hamilton, J.C. Savidis, Characterisation of Thermoplastic Liners for Steel Pipes, in: Proceedings of Aspect'96: Advances in Subsea Pipeline Engineering and Technology, Society of Underwater Technology, 1996.
[11] B. Flaconneche, J. Martin, M.H. Klopffer, Permeability, diffusion and solubility of gases in polyethylene, polyamide 11 and poly (vinylidene fluoride), Oil Gas. Sci. Technol. 56 (3) (2001) 261–278.
[12] Technical Note 814-TN, Engineering Considerations for Temperature Change. Perfomance Pipe, A division of Chevron Phillips Chemical Company LP.
[13] Final Supplemental Environmental Impact Statement for the Keystone XL Project Executive Summary January 2014 – Apendix S, United States Department of State Bureau of Oceans and International Environmental and Scientific Affairs, January 2014.
[14] J.C. Boot, I. Toropova, A.A. Javadi, Predicting the creep lives of thin-walled cylindrical polymeric pipe linings subject to external pressure, Int. J. Solids Struct. 40 (2003) 7299–7314.
[15] J.C. Boot, A.J. Welch, Creep buckling of thin-walled polymeric pipe linings subject to external ground water pressure. International, J. Thin-Walled Struct. 24 (1996) 191–210.
[16] R.M. Bakeer, M.E. Barber, S.E. Pechon, J.E. Taylor, S. Chunduru, Buckling of HDPE liners under external uniform pressure, J. Mater. Civ. Eng. 11 (4) (1999) 353–361.
[17] F. Rueda, J.P. Torres, M. Machado, P.M. Frontini, J.L. Otegui, External pressure induced buckling collapse of high density polyethylene (HDPE) liners: FEM modeling and predictions, Thin-Walled Struct. 96 (2015) 56–63.
[18] F. Rueda, J.P. Torres, P.M. Frontini, Constitutive modeling and computational simulations of the external pressure induced buckling collapse of high density polyethylene (hdpe) liners, in: Proceedings of 13th International Conference on Fracture, Beijing, China, June 2013.
[19] J.S. Bergström, J.E. Bischoff, An advanced thermo-mechanical constitutive model for UHMWPE, international, J. Struct. Chang. Solids (2010) 31–39.
[20] D. Glock, Behavior of Liners for Rigid Pipeline Under External Water Pressure and Thermal Expansion, English translation, Der Stahlban, 1997, vol. 7, pp. 212–217.
[21] J. F. Mason, P. Dang, F. Gerard, Design Analysis of Polyamide 11 Liners: Operating Higher than the Critical Buckling Pressure, in: Proceedings of Corrosion 2004, NACE International.
[22] S. Kyriakides, L.H. Lee, Buckle propagation in confined steel tubes, Int. J. Mech. Sci. 47 (4) (2005) 603–620.
[23] K.M. El-Sawy, Inelastic stability of tightly fitted cylindrical liners subjected to external uniform pressure, Thin-Walled Struct. 39 (9) (2001) 731–744.
[24] J.C. Boot, Elastic buckling of cylindrical pipe linings with small imperfections subject to internal pressure, Trench. Technol. Res. 12 (1998) 3–15.
[25] J.C. Boot, A.A. Javadi, I.L. Toropova, The structural performance of polymeric linings for nominally cylindrical gravity pipes, Thin-Walled Struct. 42 (2004) 1139–1160.
[26] J.C. Boot, M.M. Naqvi, The structural characterization of corrosion-resistant linings for hydrocarbon pipelines, in: Proceedings of Corrosion 2000, NACE International.
[27] J.F. Mason, E. Pinel, G. O'Brien, Experimental investigation of buckling in highly aged polyamide 11 liners, in: Proceedings of Corrosion 2004, NACE International.
[28] S.R. Frost, A.M. Korsunsky, Wu Y-S, A.G. Gibson, 3-D Modeling of liner collapse, in: Proceedings of Conference NACE, 2000.
[29] E. Pinel, J. Mason, G. O'Brien, Experimental investigation of buckling in highly aged polyamide-11 liners, Corrosion (2004), paper nro. 04713.
[30] K. El-Sawy, I.D. Moore, J Struct. Eng. 124 (1998) 1350–1358.
[31] K.M. El-Sawy, A.L. Elshafei, Neural network for the estimation of the inelastic buckling pressure of loosely fitted liners used for rigid pipe rehabilitation, Thin-Walled Struct. 41 (8) (2003) 785–800.
[32] R.J. Young, P.A. Lovell, Introduction to Polymers, 2nd ed., Chapman & Hall, London 1991, pp. 310–393.
[33] F. Rueda, J.L. Otegui, P.M. Frontini, Numerical tool to model collapse of polymeric liners in pipelines, Eng. Fail. Anal. (2011) 24–33.
[34] D. Lebsack, R. Egner, D. Hawn, Extending liner installation lengths, in: Proceedings of Corrosion 2004, NACE International.
[35] ASTM D638-03, Standard Test Method for Tensile Properties of Plastics, American Society for Testing and Material, Philadelphia, PA.
[36] ASTM D0695-02A, Standard Test Method for Compressive Properties of Rigid Plastics, American Society for Testing and Material, Philadelphia, PA.
[37] J.S. Bergström, C.M. Rimnac, S.M. Kurtz, An augmented hybrid constitutive model for simulation of unloading and cyclic loading behavior of conventional and highly crosslinked UHMWPE, Biomaterials (2004) 2171–2178.
[38] PolyUMod, A Library of Advanced User Materials v. 2.4.2, User's Manual. ©Veryst Engineering LLC, 2013.
[39] J. Bergstrom, Introduction to MCalibration, Software Tutorial, Veryst Engineering LLC, ⟨www.veryst.com⟩, 2013.
[40] J.A. Nelder, R. Mead, A simplex method for function minimization, Comput. J. 7 (1965) 308–313.
[41] Abaqus Analysis User´s Manual, 2010, Section 11.5.1, DassaultSystèmes, 2010.
[42] S.R. Frost, A.M. Korsunsky, Y.S. Wu, A.G. Gibson, 3-D Modelling of liner collapse, Corrosion 00779 (2000).